

A Methodology for Transformer Ratio Adjustment in Small-Size Rotary Transformers

Saeed Hajmohammadi, MohammadSadegh KhajueeZadeh, Farid Tootoonchian, *Senior, IEEE*, and Sajjad Mohammadi, *Member, IEEE*

Abstract—This study addresses a neglected challenge that has been hidden in the Rotary Transformer (RT) field: the possibility of a discrepancy between transformer ratio and turn number ratio in small-size transformers. Previous investigations have shown that in the geometry design of RTs, as well as their resonant circuit design, the transformer ratio has been regarded as the same as the turn number ratio. This estimation is logical and true when a large-size RT is investigated. However, in small-size RTs, the magnitudes of leakage and magnetization inductances are significantly close, which leads to a difference between transformer ratio and turn number ratio. Accordingly, the absence of an exact methodology for transformer ratio calculation brought us to conduct this investigation. In this regard, a transformer ratio adjustment is suggested after proposing a low-error magnetic model. Its accuracy is high enough to consider different air gaps and subsequently calculate inductance with reference to 3D finite element analysis (3D-FEA). Finally, we take advantage of a test bench to show the exactness and proficiency of the suggested transformer ratio adjustment.

Index Terms—Rotary transformer, transformer ratio, magnetic model, small-size transformer, finite element analysis.

I. INTRODUCTION

IN rotary machinery with rotor excitation, such as doubly-fed induction generators [1] and wound-rotor synchronous machines [2], as well as resolvers [3], providing a reliable manner to transfer energy and data between the stationary and rotary sides will offer different choices. The first illustration of electric excitation rotors is the set of slip rings and brushes, which cause a significant amount of friction loss. Since they wear out over time, they release carbon inside the motor box, leading to a higher possibility of fire and less safety factor [1]. Hence, scholars have made an effort to find reliable alternatives. Rotary Transformers (RTs) are at the center of attention as a promising choice to substitute brushes, which not only solve the safety challenge but also suggest lower maintenance costs and smaller installation sizes [4]. The initial idea of RT originates from stationary transformers; both works

based on electromagnetic induction, providing them with a merit for short-distance energy transmission [5]. In RT, as evident from its name, an air gap exists between the primary and secondary windings to enable rotary side movement, keyed on the shaft. The primary side is fixed and known as stationary with a connection to the excitation supply.

Since the permeability of air is smaller than that of the magnetic core, the amount of energy storage in the air gap is high, leading to a negative effect on the magnitude of magnetization inductance and subsequently providing the transformer with higher and non-negligible leakage inductance [1]. Accordingly, the primary winding will sustain a higher current than a similar winding in a stationary transformer due to high magnetization current and reflection of secondary current, simultaneously. Consequently, in RT, the resistive loss is higher [6]. Moreover, high leakage inductance is synonymous with high magnetic flux loss as a series element in the transformer circuit. The leakage inductance will store a significant amount of current and release it, resulting in high stress on switches in addition to voltage fall on both sides [5]. Taking advantage of resonant circuits, rather than snubber circuits, can appropriately address these challenges, such as switches' commutation in zero contemporary voltage and current [7]. On the other hand, the leakage is not constant for different geometries [8]. Thus, transformer redesign is necessary to fulfill size constraints and preliminary conditions in zero voltage transition [8]. We face an equality, on one hand, of leakage inductance as a function of geometry, and on the other hand, leakage as a function of resonant tank frequency [7]. In the following of transformer design to meet the aim of its installation size, magnetization, and leakage inductances will be taken into account. Subsequently, the frequency must be chosen in line with total losses minimization [5]. Moreover, voltage fall is another negative effect of leakage emergence, which is synonymous with lower energy transfer capability [7]. Since decisions have been made about geometry and frequency, the freedom now lies in flux density maximization, which has a direct relation to the transformer ratio [9].

In line with such background knowledge, different designs have been suggested with a change in magnetic core, relative location of windings, and their collection inside the slots [3], [5], [6], [8], [10]–[17]. In [15], a new topology was suggested that offers benefits such as high angular velocity, low centrifugal stress, low core loss, low prototype tolerance, high energy transfer capability, and low leakage inductance. However, its airgap length is large. Such advantages are due to

Saeed Hajmohammadi, MohammadSadegh KhajueeZadeh, and Farid Tootoonchian are with the Electrical Engineering Department, Iran University of Science and Technology, Tehran 11155-8639, Iran (e-mail: s.hajmohammadi1994@gmail.com; mohammadkhajuee@yahoo.com; tootoonchian@iust.ac.ir).

Sajjad Mohammadi is with the Department of Electrical Engineering and Computer Science, Massachusetts Institute of Technology, Cambridge, MA 02139 USA (e-mail: sajjadm@mit.edu).

the use of a lightweight non-magnetic and non-conductive rotor core, a series-series resonant circuit, and a winding configuration of primary-secondary-primary. In [10], [13], [16], we observe a trend towards disintegrated ferrite I or U cores in RT, rather than integrated cores [5], [6], [15], due to their lighter weight, better thermal conditions, and lower core loss. The first generation of these topologies was column magnetic cores (I cores), which suffer from magneto-resistance changes and high leakage flux. In [16], modifications to the geometry, such as yoke and teeth lengths, were made to achieve maximum magnetization and minimum leakage inductance. However, longer yoke and teeth lengths can lead to small window for winding and high risk of iron teeth saturation. Additionally, the inner corner of the rotor teeth is smaller than the outer corner, which exacerbates saturation risk. To address this issue, a shift distance was also regarded as a modification to balance corner saturations. Since ferrite U cores serve as the base for this topology, it suffers from oscillation in magnetization inductance. In [10], it was shown that a slight difference in height of U cores can enhance magneto-resistance in areas with loose magnetic flux bond. In [10], primary cores are shorter, while in [13], primary cores are longer, providing the design with a higher magnetic flux bond and lighter weight.

One of the most highlighted shortages that airgap brings about is the low misalignment tolerance. In other words, a small installation error is synonymous with a large degradation in voltage gain due to the significant change in inductances. In [12], a single-emission configuration was designed to address this challenge, which did not have a whole ring as the stator core; less possibility of collision between different edges. This configuration has merits such as higher angular velocity, higher safety, and lower prototype cost. In [11], a multi-emission configuration, which is an analogous idea to [12] about a not-whole core, was suggested; significant misalignment tolerance was gained.

However, a condition that can undermine the exactness of all the above designs is the size of the transformer. If the transformer is small, similar to a signal transformer in resolvers, the main conclusion about the equality of transformer ratio and turn numbers ratio will not be met due to the close magnitudes of magnetization and leakage inductances. If we want to discuss this in detail, the transformer ratio has a direct effect on geometry design, and as a domino effect, it will affect the exactness of resonant circuit calculations; at the end, this can lead to a mistaken grasp of loss levels and voltage gain.

In the following, providing an overview of transformer circuit models and introduce the case study are the main aim

of section II. Additionally, the cause of transformer ratio mismatch is shown through Bode diagrams, highlighting the necessity of proposing an exact methodology for transformer ratio calculation. In section III, a low-error magnetic model is suggested for transformers, particularly for inductance calculation. The accuracy of this magnetic model is analyzed with reference to 3D finite element analysis (3D-FEA), and the results confirm its exactness. Finally, a methodology for transformer ratio adjustment is suggested, and its proficiency is shown through Bode diagrams. In the last section, the suggested methodology's exactness is investigated experimentally.

II. PRELIMINARIES

A. Electrical Equivalent Circuit

First and foremost, this section delves into a review of different circuit models for transformers, which enables a thorough grasp of the transformer ratio and serves as a preliminary for section III.

1) Model I

This circuit models the transformer as a set of self and mutual inductances [16], as shown in Fig. 1a. Here, r_s is resistance on the stator-side or primary resistance, l_{ss} denotes the self-inductance of the stator side, and i_s and v_s symbolize the current and voltage on the stator side. Likewise, the index of r symbolizes the rotor-side, such as r_r , l_{rr} , i_r , and v_r . Additionally, m denotes the mutual inductance. Based on the given definition, the flux linkage of the rotor and stator sides, as well as their voltages, can be written as follows [16]:

$$\begin{cases} \lambda_s = l_{ss}i_s + mi_r \\ \lambda_r = mi_s + l_{rr}i_r \end{cases} \quad (1)$$

$$\begin{cases} v_s = r_s i_s + d\lambda_s/dt \\ v_r = r_r i_r + d\lambda_r/dt \end{cases} \quad (2)$$

Through 3D-FEA, the inductance matrix will be generated, with no distinction between leakage and magnetization inductances.

$$L = \begin{bmatrix} l_{ss} & m \\ m & l_{rr} \end{bmatrix} \quad (3)$$

2) Model II

Since the basis of transformer and resonant circuit design is magnetization and leakage inductances, providing a circuit that can show their roles in the transformer circuit diagram offers benefits. According to this logic, Fig. 1b shows the disintegrated terms of leakage inductance for both stator and rotor sides (l_{ls1} and l_{lr1}). Additionally, this circuit models the magnetization inductance (l_{m1}) as a single branch on the primary side. If we want to obtain analogous behavior from

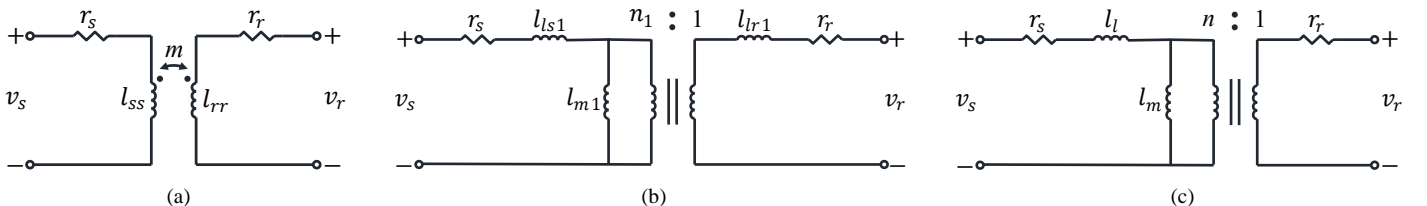


Fig. 1. Circuit models of transformer.

$$H_T = \frac{v_r}{v_s} = \frac{mz_l s}{(l_s(m+l_r)+ml_r)s^2+(r_s(m+l_r)+(m+l_s)(z_l+r_r))s+r_s(z_l+r_r)} \quad (10)$$

$$H_{Tr1} = \frac{v_r}{v_s} = \frac{l_{m1}z_l' s/n_1}{(l_{s1}(l_{m1}+l_{lr1}')+l_{m1}l_{lr1}')s^2+(r_s(l_{m1}+l_{lr1}')+(l_{m1}+l_{s1})(z_l'+r_r'))s+r_s(z_l'+r_r')} \quad (11)$$

$$H_{Tr2} = \frac{v_r}{v_s} = \frac{l_m z_l' s/n}{l_l l_m s^2+(r_s l_m+(l_m+l_l)(z_l'+r_r'))s+r_s(z_l'+r_r')} \quad (12)$$

the circuit in Fig. 1b with the base circuit in Fig. 1a, we can define its inductances (l_{s1} , l_{lr1} , and l_{m1}) as follows, where n_1 is the transformer ratio and k is the coefficient of coupling.

$$n_1 = 1/\sqrt{l_{rr}/l_{ss}} \quad (4)$$

$$l_{s1} = (1-k) * l_{ss} \quad (5-1)$$

$$l_{lr1} = (1-k) * l_{rr} \quad (5-2)$$

$$l_{m1} = k * l_{ss} \quad (5-3)$$

3) Model III

In Fig. 1c, the circuit models the leakage inductance as an integrated term on the stator side (l_l). According to the circuit in Fig. 1c, the inductance matrix will be regenerated as given in (6). This will be regarded the same as (3) if we want to obtain an analogous behavior with the base circuit in Fig. 1a. Therefore, the transformer ratio and inductances will be written as (8) and (9):

$$L = \begin{bmatrix} l_{ss} & l_{s,r} \\ l_{r,s} & l_{rr} \end{bmatrix} = \begin{bmatrix} l_l + l_m & l_m/n \\ l_m/n & l_m/n^2 \end{bmatrix} \quad (6)$$

$$k = \sqrt{l_{s,r}l_{r,s}/l_{ss}l_{rr}} = \sqrt{l_m/(l_m + l_l)} \quad (7)$$

$$n = l_{s,r}/l_{rr} = k/\sqrt{l_{rr}/l_{ss}} \quad (8)$$

$$l_m = n l_{s,r} \quad (9-1)$$

$$l_l = l_{ss} - l_m \quad (9-2)$$

B. Case Study

Axial flux configuration [18] is designed to comply with the shaft length limitation, and has a dependency on the dimensions of the motor's end windings [19]. In this configuration, both sides are arranged in back-to-back rings. Fig. 2 and Table I show the geometry and geometrical dimension data of this configuration for large- and small-size transformers.

C. Bode Diagram

Bode diagram can be used to confirm (4)-(9); therefore, the rotor-to-stator voltage ratio can be written as (10)-(12) for each circuit. In this case, z_l is a 10 Ohm resistance and $s = j\omega$. Consistent with Fig. 3, a good agreement is seen between the curves, which corroborates (4)-(9). Moreover, the 3D-FEA is the main tool to calculate the self and mutual inductances of transformers, with reference to the circuit diagram of Fig. 1a. Thereafter, leakage and magnetization inductances of circuit diagrams in Fig. 1c are on hand, proceeding from what is written in (6)-(9); as shown in Table II.

D. Problem Description

According to the data given in Table II, it is clear that transformer ratio and turn-number ratio are not the same, particularly for small-size/signal transformers. This difference arises from the significant closeness in the magnitudes of leakage and magnetization inductances, as evident in the Bode

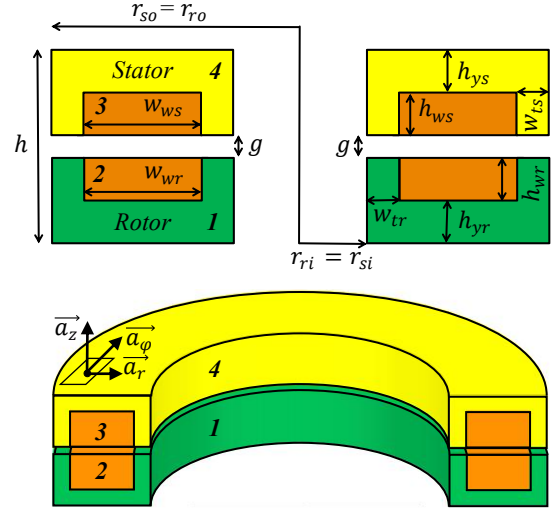


Fig. 2. Details of transformer geometry: (1) rotor core, (2) rotor winding, (3) stator winding, and (4) stator core.

TABLE I
THE GEOMETRICAL DIMENSION DATA

Parameters	Axial Small-Size	Axial Large-Size
h_{ws}/h_{wr}	3.5mm/3.5mm	7.8mm/7.8mm
w_{ws}/w_{wr}	5.5mm/5.5mm	35.6mm/35.6mm
r_{si}/r_{ri}	13mm/13mm	17mm/17mm
r_{so}/r_{ro}	21.5mm/21.5mm	67.6mm/67.6mm
g	0.6mm	0.6mm
w_{ts}/w_{tr}	1.5mm/1.5mm	7.5mm/7.5mm
h_{ys}/h_{yr}	1.5mm/1.5mm	7.5mm/7.5mm
turn number ratio	1	1

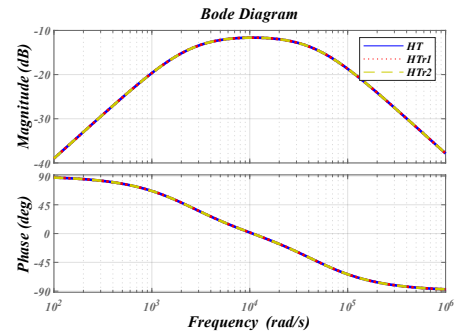


Fig. 3. Bode diagrams for circuit models of transformer: H_T (Fig. 1a), H_{Tr1} (Fig. 1b), and H_{Tr2} (Fig. 1c).

TABLE II
PARAMETERS OF CIRCUIT MODELS

Model Parameters	Axial Small-Size	Axial Large-Size
l_{ss}	3.322mH	4.693H
l_{sr}	2.968mH	4.625H
l_{rr}	3.348mH	4.695 H
l_l	0.6915mH	0.137H
l_m	2.631mH	4.556H
n	0.887	0.985
turn number ratio	1	1

$$l_m = \frac{N_s^2}{R_m}$$

$$R_m = R_{ys} + R_{yr} + R_{ts1} + R_{tr1} + R_{cs1} + R_{cr1} + R_{g,eq1} + R_{ts2} + R_{tr2} + R_{g,eq2} + R_{cs2} + R_{cr2} \quad (13)$$

$$R_{g,eq} = R_{g,i}R_gR_{g,o}/R_{g,i}R_g + R_{g,o}(R_{g,i} + R_g)$$

$$R_{g,x} = R_{f,x}R_{sh,x}/R_{f,x} + R_{sh,x}$$

diagrams of Fig. 4(a); negligible in large-size transformers, as shown in Fig. 4(b). In Figs. 3 and 4, the basis is the circuit investigated in Fig. 1a. This highlights the absence of a general methodology for transformer ratio calculation in the case of small-size transformers.

III. PROPOSED METHOD

A. Magnetic Equivalent Circuit (MEC)

Magnetic models define the correlation between the geometry of a transformer and its circuit model; a concentration on magnetization and leakage inductances.

1) Magnetization Inductance

Fig. 5 is the magnetic circuit, which takes into account the fringe reluctance. In this regard, the magnetization inductance (l_m) can be written as follows, where R_m is the reluctance of the main magnetic flux, and R_{ts} , R_{tr} , R_{ys} , R_{yr} , R_{cs} , and R_{cr} are the tooth, yoke, and corner reluctances of the stator and rotor. Here, the indices of t , y , and c symbolize the tooth, yoke, and corner. Moreover, $R_{g,eq}$ denotes the reluctance of airgap flux, and N_s is the number of turns on the stator side.

According to (13), in addition to R_g , which accounts for the airgap flux in a straight line, $R_{g,o}$ and $R_{g,i}$ are also regarded to account for the fringe effect. In general, (14) is the core of the next calculations, where dl , H , B , and μ are in order an increment, magnetic field strength, magnetic flux density, and the medium's permeability. In Fig. 6, flux tubes are also shown, which form the basis of integrals in (14)-(24).

$$R = \frac{mmf}{flux} = \frac{\int \vec{H} \cdot d\vec{l}}{\iint \vec{B} \cdot d\vec{S}} = \int \frac{dl}{\mu S} \quad (14)$$

According to Cylindrical coordinate system (r, φ, z) in Fig. 2 and Fig. 6, R_{ys} will be written as an instance below, where the increment is in the direction of \vec{a}_r .

$$R_{ys} = \int_{r_{si}+w_{ts}}^{r_{so}-w_{ts}} \frac{dr}{\mu 2\pi r h_{ys}} = \ln\left(\frac{r_{so}-w_{ts}}{r_{si}+w_{ts}}\right) / \mu 2\pi h_{ys} \quad (15)$$

In the same manner, other reluctances can be written as:

$$R_{yr} = \ln\left(\frac{r_{ro}-w_{tr}}{r_{ri}+w_{tr}}\right) / \mu 2\pi h_{yr} \quad (16)$$

$$R_{ts1} = h_{ws} / \mu \pi ((r_{si} + w_{ts})^2 - r_{si}^2) \quad (17-1)$$

$$R_{ts2} = h_{ws} / \mu \pi (r_{so}^2 - (r_{so} - w_{ts})^2) \quad (17-2)$$

$$R_{tr1} = h_{wr} / \mu \pi ((r_{ri} + w_{tr})^2 - r_{ri}^2) \quad (18-1)$$

$$R_{tr2} = h_{wr} / \mu \pi (r_{ro}^2 - (r_{ro} - w_{tr})^2) \quad (18-2)$$

$$R_{g1} = g / \mu_0 \pi ((r_{ri} + w_{ts})^2 - r_{ri}^2) \quad (19-1)$$

$$R_{g2} = g / \mu_0 \pi (r_{ro}^2 - (r_{ro} - w_{tr})^2) \quad (19-2)$$

$$R_{cs,r} = \frac{1}{4\mu((r_{so} - w_{ts}) \ln\left(\frac{r_{so}}{r_{so} - w_{ts}}\right) + w_{ts})} \quad (20)$$

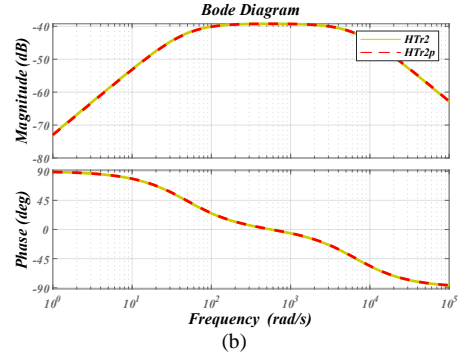
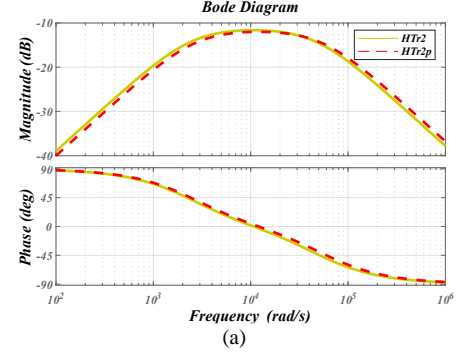


Fig. 4. Bode diagrams for transformer circuit model in Fig. 1a, where H_{Tr2} denotes exact transformer ratio, and H_{Tr2p} denotes turn number ratio: (a) small-size transformer, and (b) large-size transformer.

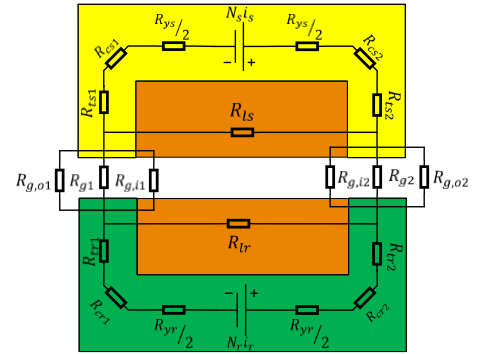


Fig. 5. Magnetic circuit of the rotary transformer.

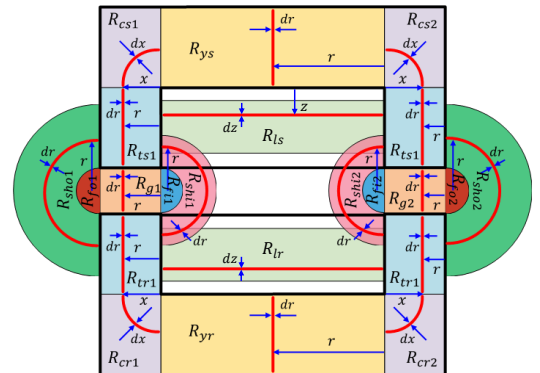


Fig. 6. Paths of integrations and flux tubes of the rotary transformer.

To calculate the fringe effect in a magnetic circuit, (14) remains effective, but with a change in S and dl for R_{sh} .

$$R_{sh,o} = \left(\int_{\frac{g}{2}}^{r_{f,o} - \frac{g}{2}} \frac{\mu_0 L_x}{\pi r} dr \right)^{-1} \quad (21-1)$$

$$R_{sh,i} = \left(\int_{\frac{g}{2}}^{r_{f,i} - \frac{g}{2}} \frac{\mu_0 L_x}{\pi r} dr \right)^{-1} \quad (21-2)$$

Where L_x is different between the inner and outer radius of the transformer, as shown in Fig. 7. Furthermore, in accordance with [20], R_f is written as below:

$$R_{f,io} = 1/0.26\mu_0 L_x \quad (22)$$

According to (21), r_f changes with geometry and location of the fringes. Thus, in [21] an effort was made to address this challenge through the radius definition of fringe fluxes on both the outer and inner walls of the transformer, regarding 3D-FEA as a metric of exactness. In agreement with [21], the outer radius ($r_{f,o}$) should be chosen to be the same as (23-1). For the inner fringe, which is much smaller than the outer one, it is better to choose the inner radius ($r_{f,i}$) as written in (23-2).

$$r_{f,o} = h - (h_{wr} + h_{yr}) \quad (23-1)$$

$$r_{f,i} = \min \left(\left(h - (h_{wr} + h_{yr}) - h_{ys} \right), \frac{w_{ws}}{2} \right) \quad (23-2)$$

According to Figs. 6 and 7, $R_{g,o}$ and $R_{g,i}$ are as shown below:

$$R_{g,o2} = 1/2\mu_0 r_{si} \left(0.26\pi + \ln \frac{r_{f,o} - \frac{g}{2}}{\frac{g}{2}} \right) \quad (24-1)$$

$$R_{g,i2} = 1/2\mu_0 (r_{si} + w_{ts}) \left(0.26\pi + \ln \frac{r_{f,i} - \frac{g}{2}}{\frac{g}{2}} \right) \quad (24-2)$$

$$R_{g,o1} = 1/2\mu_0 r_{so} \left(0.26\pi + \ln \frac{r_{f,o} - \frac{g}{2}}{\frac{g}{2}} \right) \quad (24-3)$$

$$R_{g,i1} = 1/2\mu_0 (r_{so} - w_{ts}) \left(0.26\pi + \ln \frac{r_{f,i} - \frac{g}{2}}{\frac{g}{2}} \right) \quad (24-4)$$

2) Leakage Inductance

When magnetic flux links one winding in a transformer, but not the other, such flux contributes to leakage inductance. According to Fig. 8(a), in regions I and III, the flux leakage lines almost seem as aligned lines within the windows, with a height that is the same as the window width of the transformer (w_w). In region II, due to the air gap effect, the flux leakage lines traverse a longer length than the window width of the transformer, which is in contrast to what was taken in [8], as shown in (29) and Fig. 8(a). If we treat it in the same manner as what was shown in [8], the magnetic model will not have enough exactness in the face of leakage inductance, especially in larger air gaps. In other words, the leakage inductance will rise more than what is happening in 3D-FEM. Owing to the lack of an exact estimation of S for flux leakages, (14) will not work here. Accordingly, we can define leakage inductance as an integral of magnetic energy density over the volume of the winding in the transformer window (v_w), as shown below. In this case, the leakage inductance, as in Fig. 1c, is an integrated term on one side, either the stator or rotor. Here, I_s denotes the stator current.

$$\frac{1}{2} l_l (I_s)^2 = \iiint_0^{v_w} \frac{1}{2} BH dv = \iiint_0^{v_w} \frac{1}{2} \mu_0 H^2 dv \quad (25)$$

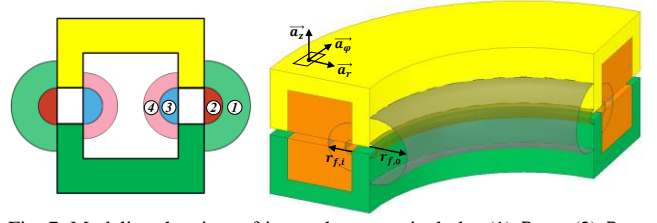


Fig. 7. Modeling the airgap fringe reluctances includes (1) $R_{sh,o}$, (2) $R_{f,o}$, (3) $R_{sh,i}$, and (4) $R_{f,i}$. It is worth to mention that L_x differs between outer and inner regions, where it is $2\pi r_i$ and $2\pi(r_i + w_{ts})$, respectively. Analogous treatment can be regarded to other regions.

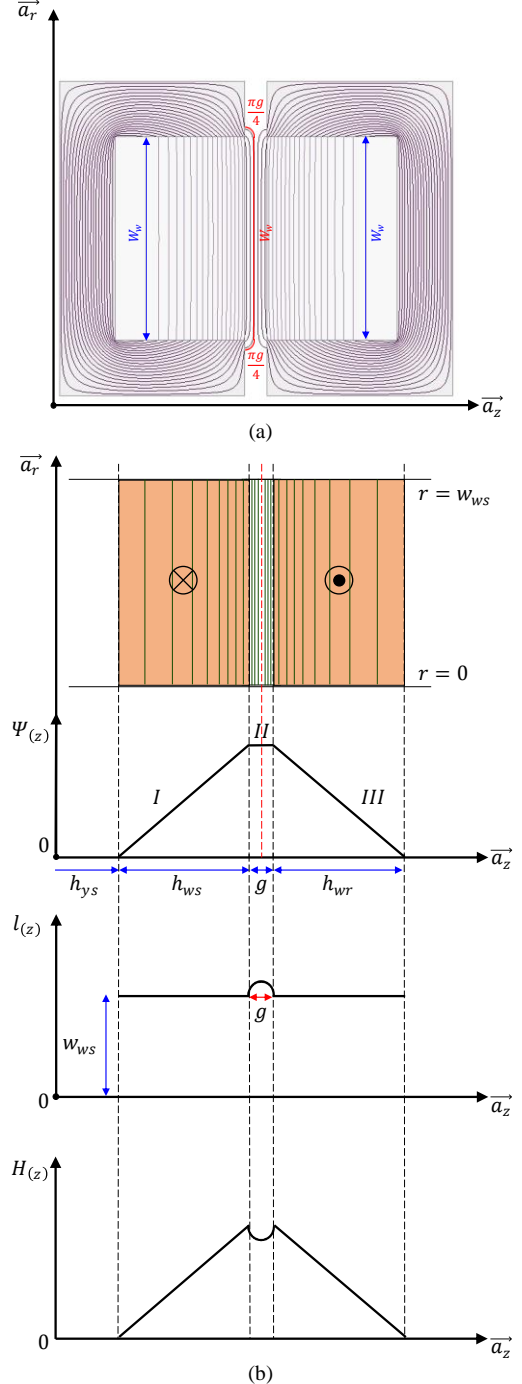


Fig. 8. (a) Flux leakage lines, and (b) leakage magnetomotive force (MMF) diagram and magnetic field strength.

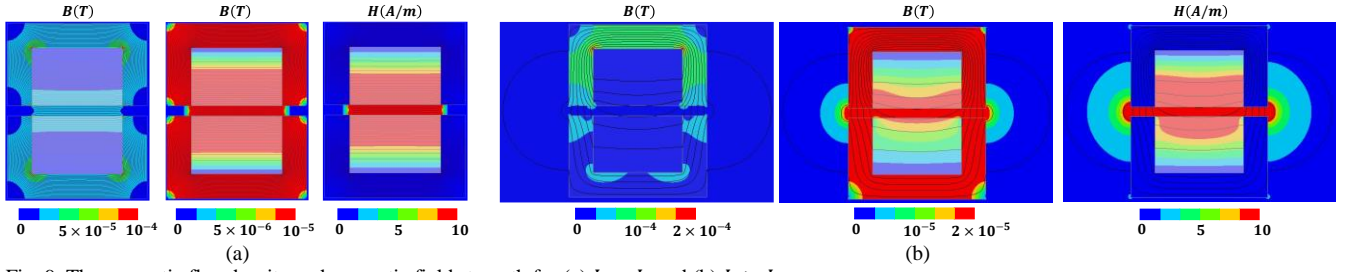


Fig. 9. The magnetic flux density and magnetic field strength for (a) $I_s = I_r$ and (b) $I_s > I_r$.

If we define H as follows, leakage inductance is written as shown in (27). Here, $\Psi(z)$ denotes the Magnetomotive Force (MMF).

$$N_s I_s = N_r I_r \quad (26-1)$$

$$\oint \vec{H} \cdot d\vec{l} = \Psi(z) \quad (26-2)$$

$$l_l = \frac{\mu_0}{(I_s)^2} \iiint_0^{v_w} \left(\frac{\Psi(z)}{l(z)} \right)^2 dv \quad (27)$$

According to $N_s I_s = N_r I_r$, the MMF distribution across the cross-section of the stator- and rotor-side windings is as shown in Fig. 8(b).

$$\Psi_{(z)\text{-Region I}} = \frac{N_s I_s}{h_{wr}} (z - h_{yr}) \quad (28-1)$$

$$\Psi_{(z)\text{-Region II}} = N_s I_s \quad (28-2)$$

$$\Psi_{(z)\text{-Region III}} = \frac{N_s I_s}{h_{ws}} (-z + h_{yr} + h_{wr} + g + h_{ws}) \quad (28-3)$$

Where, region I is between h_{yr} and $h_{yr} + h_{wr}$, region II is between $h_{yr} + h_{wr}$ and $h_{yr} + h_{wr} + g$, and region III is between $h_{yr} + h_{wr} + g$ and $h_{yr} + h_{wr} + g + h_{ws}$. According to Fig. 8(b), $l(z)$ is written as below:

$$l_{(z)\text{-Region I}} = w_{ws} \quad (29-1)$$

$$l_{(z)\text{-Region II}} = w_{ws} + \frac{\pi g}{2} \quad (29-2)$$

$$l_{(z)\text{-Region III}} = w_{ws} \quad (29-3)$$

If we substitute (28) and (29) into (27), we obtain leakage inductance as written (30).

$$l_l = \mu_0 \pi N_s^2 (r_{si} + r_{so}) \left(\frac{h_{wr}}{3w_{ws}} + \frac{h_{ws}}{3w_{ws}} + \frac{g}{w_{ws} + \frac{\pi g}{2}} \right) \quad (30)$$

B. Accuracy of MEC

According to the nature of the airgap, a larger airgap results in lower magnetization inductance and larger leakage inductance. Therefore, we should evaluate the sensitivity of the magnetic model to different airgap sizes. In this context, an airgap range of 0.4 mm to 4 mm was chosen, and 3D-FEA was regarded as the reference. In Fig. 9, the magnitudes of magnetic flux density and magnetic field strength along with the magnetic flux lines are shown. Moreover, the schematic of the mesh grid and its quality is shown in Fig. 10. The results shown in Figs. 11(a) and (b) indicate a high level of agreement between the suggested magnetic model and 3D-FEA for both inductances (Magnetization and Leakage). Thus, we can claim that the suggested magnetic model has more than 95% accuracy with an almost constant error in different airgaps.

C. Transformer Ratio Adjustment

According to the circuit shown in Fig. 1c, the transformer ratio has been written as below:

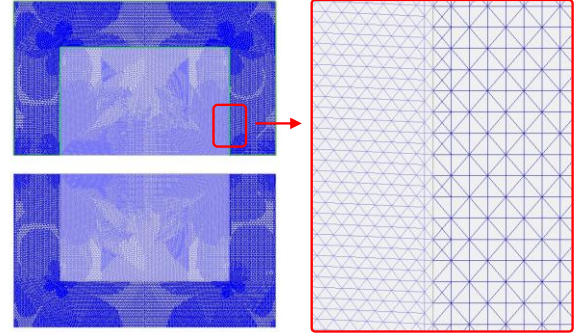


Fig. 10. The schematic of the mesh grid.

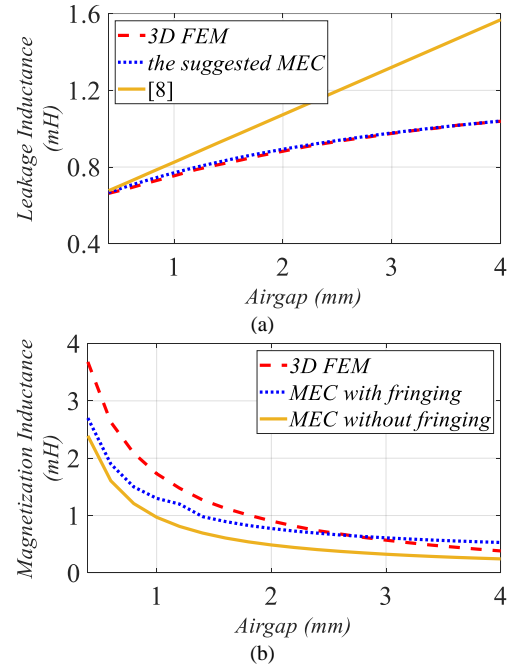


Fig. 11. (a) Leakage inductances from 3D-FEA, the investigated methodology in [8], and the suggested MEC in this study. (b) Magnetization inductances from 3D-FEA, MEC with fringing effect, and MEC without fringing effect.

TABLE III
COMPARISON OF EXACT AND ADJUSTED TRANSFORMER RATIOS FOR DIFFERENT TURN NUMBER RATIOS

Model Parameters	Turn number ratio		
	0.5	1	2
l_{ss}	830.567 μ H	3.322mH	3.322mH
l_{sr}	1.484mH	2.968mH	1.484mH
l_{rr}	3.348mH	3.348mH	836.943 μ H
$n(\text{exact})$	0.443	0.887	1.773
$n(\text{adjusted})$	0.445	0.9	1.780

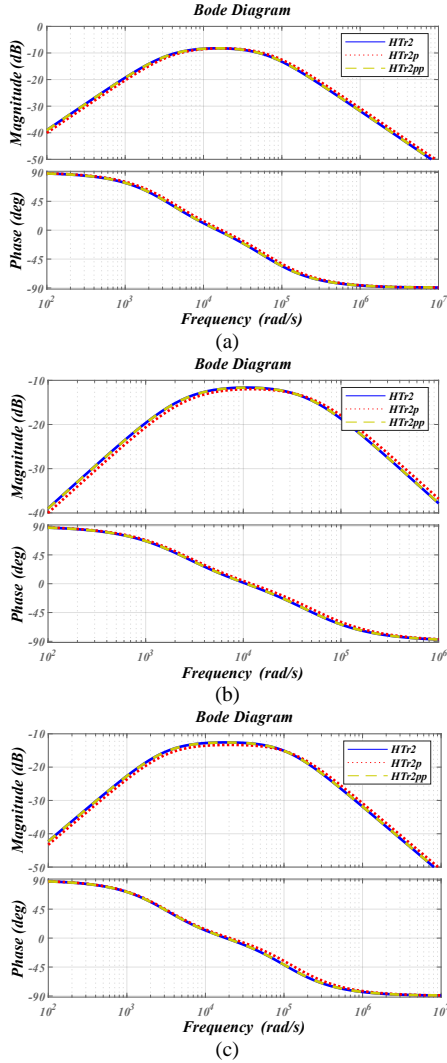


Fig. 12. Bode diagrams for different turn number ratios (a) 0.5, (b) 1, and (c) 2, where H_{Tr2} denotes the exact transformer ratio, H_{Tr2p} denotes the turn number ratio, and H_{Tr2pp} denotes the adjusted transformer ratio for transfer functions of transformer.

$$n = \sqrt{l_{s,r}l_{r,s}/l_{ss}l_{rr}} / \sqrt{l_{rr}/l_{ss}} \quad (31)$$

If we assume that $1/\sqrt{l_{rr}/l_{ss}}$ is the same as the turn number ratio, (N_s/N_r), as shown in Fig. 1b, and $\sqrt{l_{s,r}l_{r,s}} = \sqrt{l_m}$ as written in (7), then we can derive (32) as below:

$$n \cong \sqrt{\frac{l_m}{(l_m + l_i)}} \times (N_s/N_r) \quad (32)$$

In Table III, exact and adjusted transformer ratios and turn number ratios were written for different configurations according to (32). It is evident that the suggested adjustment in (32) has satisfactory accuracy. Moreover, the Bode diagrams shown in Fig. 12 also confirm this conclusion.

IV. EXPERIMENTAL MEASUREMENT

If we wish to test the proficiency of the suggested magnetic model and transformer ratio adjustment simultaneously, voltage gain (rotor- and stator-side voltages) seems to be a

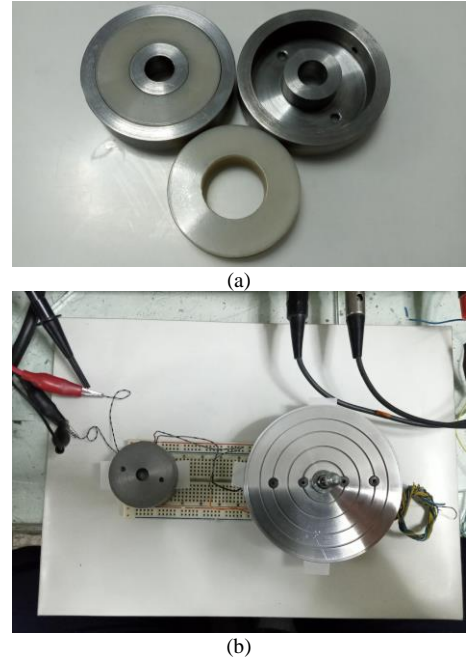


Fig. 13. The prototyped (a) rotary transformer has the same geometrical dimensions as the small-size transformer given in Table I, supplying a (b) resolver as a load.

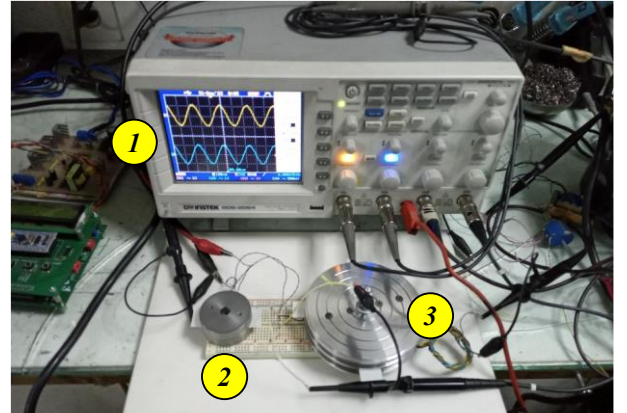


Fig. 14. Test bench with resolver load: (1) stator- and rotor-side voltages, (2) the prototyped rotary transformer, and (3) resolver as a load.

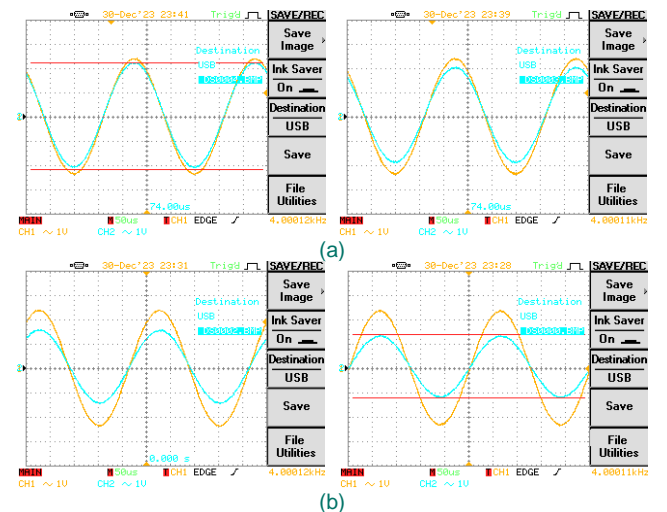


Fig. 15. The results of measurement, stator- and rotor-side voltages, for airgaps of 0.6mm (left) and 1.2mm (right): (a) No-load condition (b) resolver with $R_L = 19 \Omega$ and $L_L = 2.289 \text{ mH}$ as a load.

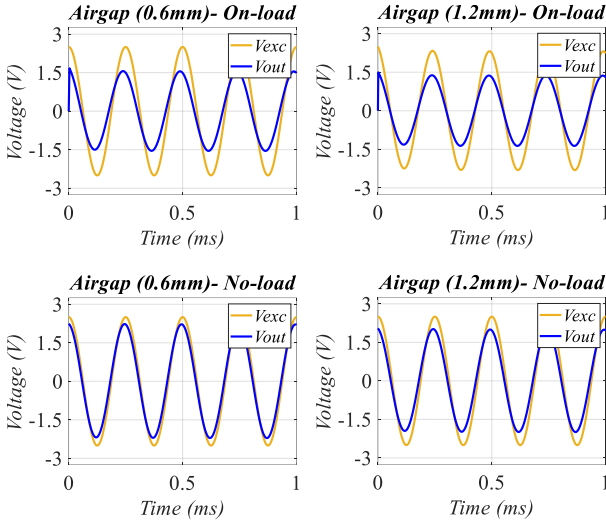


Fig. 16. The results of 3D-FEA, stator- and rotor-side voltages, for airgaps of 0.6mm and 1.2mm: on-load and no-load.

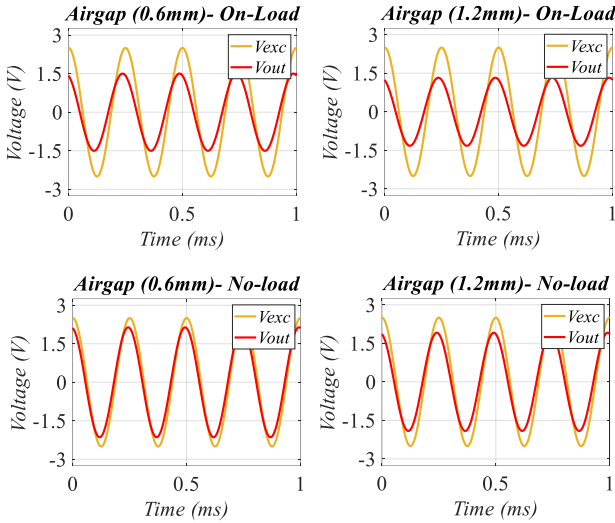


Fig. 17. The results of the circuit model in Fig. 1c, including stator- and rotor-side voltages, based on the suggested magnetic model for the calculation of leakage and magnetization inductances, as well as the suggested transformer ratio adjustment, for air gaps of 0.6mm and 1.2mm: on-load and no-load.

TABLE IV
COMPARISON OF THE SUGGESTED METHODOLOGY, 3D FEA, AND
EXPERIMENTAL MEASUREMENT

Load	Airgaps	Rotor-Side Voltages (No-Load)		
		The Suggested Methodology	3D FEA	Experimental Measurement
No-Load	0.6 mm	2.14	2.21	2.20
	1.2 mm	1.91	1.99	2.00
Resolver Load	0.6 mm	1.50	1.55	1.60
	1.2 mm	1.32	1.37	1.40

reliable method. Therefore, the investigated transformer was prototyped with the same geometrical dimensions as the small-size transformer given in Table I, as displayed in Fig. 13. The test bench is shown in Fig. 14, where a digital synthesized function generator was used for excitation with a frequency resolution of 0.1 Hz, while the magnitude of excitation voltage was adjusted with an automatic gain control circuit. The excitation voltage magnitude and frequency were

set at 2.5V and 4kHz. Moreover, the test conditions are no-load and on-load in order to determine the effect of transformer ratio adjustment. Here, a resolver with $R_L = 19 \Omega$ and $L_L = 2.289 \text{ mH}$ was regarded as the load. The test results under different loads and airgaps, stator- and rotor-side voltages, are shown in Fig. 15. Additionally, the results of stator- and rotor-side voltages of 3D-FEA and the circuit shown in Fig. 1c, when the calculation of leakage and magnetization inductances were through the suggested magnetic model, and transformer ratio was adjusted in accordance with (31), are displayed in Figs. 16 and 17. Thus, as shown in Table IV, the measurement and 3D-FEA results are in close agreement with the suggested methodology in both 0.6mm and 1.2mm airgaps. Thus, in the worst-case, the suggested methodology has less than 7% error.

V. CONCLUSION

In this work, the authors have made an effort to address a neglected but decisive issue in small-size rotary transformers: the discrepancy between transformer ratio and turn number ratio. To begin with, as preliminary, the circuit was regarded as the basis for the latter investigations, which models the leakage inductance as an integrated term on the stator side. Then, a magnetic model was suggested for the calculation of leakage and magnetization inductances, presenting higher than 95% agreement with 3D-FEA. Thereafter, transformer ratio adjustment was suggested. It was also shown that this adjustment has a decisive role in voltage gain. Finally, the investigated transformer was prototyped, and the voltage gain was regarded as a metric to verify the suggested magnetic model and transformer ratio adjustment. There was satisfactory agreement between the analyses and measurements for different air gaps.

REFERENCES

- [1] M. Ruviaro, F. Rñncos, N. Sadowski, and I. M. Borges, "Design and analysis of a brushless doubly fed induction machine with rotary transformer," in *19th International Conference on Electrical Machines, ICEM 2010*, 2010. doi: 10.1109/ICELMACH.2010.5607735.
- [2] N. Patin, E. Monmasson, and J. P. Louis, "Modeling and control of a cascaded doubly fed induction generator dedicated to isolated grids," *IEEE Transactions on Industrial Electronics*, vol. 56, no. 10, pp. 4207–4219, 2009, doi: 10.1109/TIE.2009.2028358.
- [3] M. Khazaei and F. Tootoonchian, "Comparing Different Configurations for Rotary Transformer of Wound-Rotor Resolvers," *Scientia Iranica*, vol. 0, no. 0, pp. 0–0, Aug. 2021, doi: 10.24200/sci.2021.57984.5503.
- [4] H. Zhong, C. Wu, and Y. Wang, "Design and analysis of rotary transformer for brushless doubly fed induction generators," in *Proceedings of the 13th IEEE Conference on Industrial Electronics and Applications, ICIEA 2018*, Institute of Electrical and Electronics Engineers Inc., Jun. 2018, pp. 1416–1419. doi: 10.1109/ICIEA.2018.8397931.
- [5] X. Zhu, L. Liu, and H. Qi, "Performances of a Contactless Energy Transfer System for Rotary Ultrasonic Machining Applications," *IEEE Access*, vol. 8, pp. 51981–51990, 2020, doi: 10.1109/ACCESS.2020.2978074.
- [6] S. Ditzel, A. Endruschat, T. Schriefer, A. Roskopf, and T. Heckel, "Inductive power transfer system with a rotary transformer for contactless energy transfer on rotating applications," in *Proceedings - IEEE International Symposium on Circuits and Systems*, Institute of Electrical and Electronics Engineers Inc., Jul. 2016, pp. 1622–1625. doi: 10.1109/ISCAS.2016.7538876.

- [7] X. Zhu, B. Lin, L. Liu, and Y. Luan, "Power Transfer Performance and Cutting Force Effects of Contactless Energy Transfer System for Rotary Ultrasonic Grinding," *IEEE Transactions on Industrial Electronics*, vol. 63, no. 5, pp. 2785–2795, May 2016, doi: 10.1109/TIE.2016.2514352.
- [8] H. Vardhan, M. Odavic, and K. Atallah, "Design Optimization Methodology for High-Frequency Rotary Transformers for Contactless Power Transfer Systems," in *2022 IEEE Energy Conversion Congress and Exposition, ECCE 2022*, Institute of Electrical and Electronics Engineers Inc., 2022, doi: 10.1109/ECCE50734.2022.9948210.
- [9] Chwei-Sen Wang, O. H. Stielau, and G. A. Covic, "Load models and their application in the design of loosely coupled inductive power transfer systems," in *PowerCon 2000. 2000 International Conference on Power System Technology. Proceedings (Cat. No.00EX409)*, IEEE, pp. 1053–1058, doi: 10.1109/ICPST.2000.897166.
- [10] Y. Zhou, Y. Luo, S. Liu, and D. Li, "An Efficient and Stable Embedded Multi-U-Shaped Column Rotary Transformer," *IEEE Trans Power Electron*, vol. 38, no. 5, pp. 6734–6743, May 2023, doi: 10.1109/TPEL.2023.3243211.
- [11] Z. Chen, J. Hong, Y. Zhang, Y. Kong, X. Zhao, and S. Chen, "A Contactless Energy Transfer System with High Misalignment Tolerance for Rotary Ultrasonic Machining," *IEEE Transactions on Industrial Electronics*, 2023, doi: 10.1109/TIE.2023.3283683.
- [12] Y. Luan, B. Lin, X. Ma, and X. Zhu, "Innovative Contactless Energy Transfer Accessory for Rotary Ultrasonic Machining and Its Circuit Compensation Based on Coil Turns," *IEEE Transactions on Industrial Electronics*, vol. 64, no. 10, pp. 7810–7818, Oct. 2017, doi: 10.1109/TIE.2017.2696504.
- [13] B. Ji, Y. Luo, Y. Zhou, and F. Hong, "External Embedded Multi-U-shaped Column Rotary Transformer with High Efficiency and Stability," *IEEE Trans Power Electron*, pp. 1–9, Nov. 2023, doi: 10.1109/tpe.2023.3330339.
- [14] L. Wang, J. Li, H. Nie, J. Liu, and S. Ke, "Coaxial Nested Couplers-Based Offset-Tolerance Rotary Wireless Power Transfer Systems for Electric Excitation Motors," *IEEE Access*, vol. 8, pp. 44913–44923, 2020, doi: 10.1109/ACCESS.2020.2978130.
- [15] T. Raminosoa, R. H. Wiles, and J. Wilkins, "Novel Rotary Transformer Topology with Improved Power Transfer Capability for High-Speed Applications," in *IEEE Transactions on Industry Applications*, Institute of Electrical and Electronics Engineers Inc., Jan. 2020, pp. 277–286, doi: 10.1109/TIA.2019.2955050.
- [16] Y. Zhang, J. Yang, D. Jiang, D. Li, and R. Qu, "Design, Manufacture, and Test of a Rotary Transformer for Contactless Power Transfer System," *IEEE Trans Magn*, vol. 58, no. 2, Feb. 2022, doi: 10.1109/TMAG.2021.3094135.
- [17] T. Li *et al.*, "Analysis and Design of Rotary Wireless Power Transfer System With Dual-Coupled XLC/S Compensation Topology," *IEEE Trans Ind Appl*, vol. 59, no. 2, pp. 2639–2649, Mar. 2023, doi: 10.1109/TIA.2022.3233559.
- [18] E. E. Landsman, "ROTARY TRANSFORMER DESIGN."
- [19] X. ZU and Q. JIANG, "Study of High Frequency Rotary Transformer Structures for Contactless Inductive Power Transfer," 2019 22nd International Conference on Electrical Machines and Systems (ICEMS), Harbin, China, 2019, pp. 1–5, doi: 10.1109/ICEMS.2019.8921812.
- [20] S. Mohammadi, M. Mirsalim, S. Vaez-Zadeh and H. A. Talebi, "Analytical Modeling and Analysis of Axial-Flux Interior Permanent-Magnet Couplers," in *IEEE Transactions on Industrial Electronics*, vol. 61, no. 11, pp. 5940–5947, Nov. 2014, doi: 10.1109/TIE.2014.2311391.
- [21] J. Muhlethaler, J. W. Kolar and A. Ecklebe, "A novel approach for 3d air gap reluctance calculations," 8th International Conference on Power Electronics - ECCE Asia, Jeju, Korea (South), 2011, pp. 446–452, doi: 10.1109/ICPE.2011.5944575.